Realization and simulation of high power holmium doped fiber laser for long-range transmission

Julien Le Gouët, François Gustave, Pierre Bourdon, Thierry Robin, Arnaud Laurent, Benoît Cadier

Realization and simulation of high power holmium doped fiber laser for long-range transmission

JULIEN LE GOUËT,[1,*] FRANÇOIS GUSTAVE,[1] PIERRE BOURDON,[1] THIERRY ROBIN,[2] ARNAUD LAURENT,[2] AND BENOIT CADIER [2]

[1] *Office National d'Etudes et de Recherches Aérospatiales (ONERA), Palaiseau, France*
[2] *iXblue Photonics, Lannion, France*
[*] *julien.le_gouet@onera.fr*

Abstract: We report on our realization of a high power holmium doped fiber laser, together with the validation of our numerical simulation of the laser. We first present the measurements of the physical parameters that are mandatory to model accurately the laser-holmium interactions in our silica fiber. We then describe the realization of the clad-pumped laser, based on a triple-clad large mode area holmium (Ho) doped silica fiber. The output signal power is 90 W at 2120 nm, with an efficiency of about 50% with respect to the coupled pump power. This efficiency corresponds to the state of the art for clad-pumped Ho-doped fiber lasers in the 100 W power class. By comparing the experimental results to our simulation, we demonstrate its validity, and use it to show that the efficiency is limited, for our fiber, by the non-saturable absorption caused by pair induced quenching between adjacent holmium ions.

1. Introduction

In various applications like long-range free-space optical telecommunications, wind lidar, or defense systems, the requirements of the laser source are the following: robustness to harsh environments, high average power (>100W), low thermal load, single spatial mode ($M^2 \simeq 1$), high transmission through the atmosphere, eye-safe radiation, and high electro-optic efficiency. When it comes to conciliate all these requirements, all-fiber laser sources appear as the best compromise.

Several solutions can then be considered. For example, the fiber telecommunication band offers some atmospheric transmission windows which can be addressed with an erbium-doped fiber laser, emitting between 1560 nm and 1580 nm and pumped in-band by laser diodes at 1532 nm to avoid large quantum defect [1]. However, infrared laser diodes suffer an efficiency drop at high power, due to various thermally activated loss mechanisms [2]. A thulium (Tm) fiber laser at 2 µm could also meet the requirements above, by using laser diode pumping at 793 nm [3, 4], but thermal load is expected to limit the power scaling. In-band pumping of a Tm fiber by another Tm fiber laser is an alternative, at the expense of the efficiency for laser wavelengths longer than 2050 nm [5]. In the long term perspective of scaling the power up to several kW, another promising option consists in pumping holmium (Ho) doped fibers in the ${}^5I_8 - {}^5I_7$ transition (close to 1950 nm) with a Tm fiber laser.

Since the record power of 400 W and 50% efficiency established with an all-fiber clad pumped configuration [6], this type of laser source attracted interest from a number of other laboratories [7–11]. It should be noted that other configurations can allow higher efficiency in the class of 100 W laser power (e.g. core-pumped [12] or double-end pumped [13], but these configurations are not compatible with the requirements of thermal load or robustness of a kW laser.

En route to a high power laser source based on in-band pumped Ho fibers, one of the

limitations to the efficiency lies in the silica purity, for clad and core, in terms of hydroxyl OH concentration. Indeed these impurities, whom concentration can vary with the fabrication method, present absorption bands in the spectral range around 2 µm which includes pump and signal wavelengths [14]. Another limitation to the laser efficiency in highly doped fibers stems from the pair-induced quenching, which translates at high power into a non-saturable absorption. Both contributions to the pump and signal attenuations must be precisely measured and taken into account.

In this article we resume our work, from the spectroscopy of the holmium ions in single-mode fiber (SMF) samples to the realization of a high efficiency high power laser based on a triple-clad large mode area (LMA) fiber. We compare these results to our numerical simulation of the fiber laser, based on all the physical parameters measured on the SMF samples and on the LMA fiber. We finally discuss the main limitations of efficiency in the case of our fiber laser.

2. Spectroscopy of Ho in a single-mode sample

The generation of a laser signal in a rare-earth doped fiber cavity is ruled by a set of very well-known equations for population rate and propagation [15]. To solve these equations, the following values are required: linear absorption by the active ion, cross-section spectra for absorption and emission, excited state lifetime, and propagation passive loss. In addition, high holmium concentrations allow the formation of ion pairs which can reduce the laser efficiency through non-radiative energy transfers [16, 17], so the fraction of ion pairs must be measured. The values of all these physical parameters can vary significantly with the composition of the fiber, so they must be measured in detail to permit an accurate simulation of the fiber laser.

For rare-earth ions in silica fibers, the principle of measurement of each of these parameters is quite universal and already well documented in the literature. Therefore the principle and setup are only briefly exposed. Our results are commented and compared to previous measurements, when possible.

2.1. Absorption cross-section spectra

Some values of the absorption cross-section σ_{abs} have been already published for the ${}^5I_8 - {}^5I_7$ transition of holmium in silica fibers. However the variations of fabrication process and co-dopant ratios in the core induce a strong dispersion. Here are some values of σ_{abs} at 1950 nm that are given or can be infered in the literature: 2.9 10^{-25}m^2 [18], 4.65 10^{-25}m^2 [19], 5.8 10^{-25}m^2 [20], and up to 8.5 10^{-25}m^2 [21]. Thus a specific measurement on our own samples is necessary.

The absorption cross-section at a given wavelength $\sigma_{\text{abs}}(\lambda)$ is obtained from the holmium concentration in the fiber core and from the linear absorption at λ, following the expression

$$\alpha_{\text{Ho}}(\lambda) = \sigma_{\text{abs}}(\lambda).[\text{Ho}].\Gamma(\lambda) \tag{1}$$

where $\Gamma(\lambda) = 1 - \exp\left[-2.r^2_{\text{core}}(\lambda)/w^2_{\text{mode}}(\lambda)\right]$ corresponds to the overlap integral between the fundamental mode (beam radius w_{mode}) and the active core (radius r_{core}).

We measured the linear absorption spectrum of a SMF single-clad sample (iXblue HDF-PM-8-130), by the usual cut-back method [22]. At the absorption peak wavelength $\lambda_0 = 1946$ nm, this moderately doped fiber (defined here as fiber #1) presents an absorption of 57 ± 1 dB/m. The core composition of this SMF sample was measured with a scanning electron microscope equipped for wavelength dispersive spectroscopy (WDS). The concentration profile is not strictly flat and presents a small bell shape, with an average Ho^{3+} concentration [Ho] = $(3.7 \pm 0.6)10^{25}$ m^{-3}. Since the relative difference is small compared to a step index profile (about 10% peak to peak), we consider below an effective step index doping with this average concentration. Given the fiber dimensions ($2r_{\text{core}} = 8$ µm, numerical aperture NA=0.17), the mode diameter at λ_0 is $2w_{\text{mode}} = 9.4$ µm, and the overlap parameter is $\Gamma(\lambda_0) = 0.76$. We could thus infer an absorption cross-section $\sigma_{\text{abs}}(\lambda_0) = (4.8 \pm 0.8)10^{-25}$ m^2.

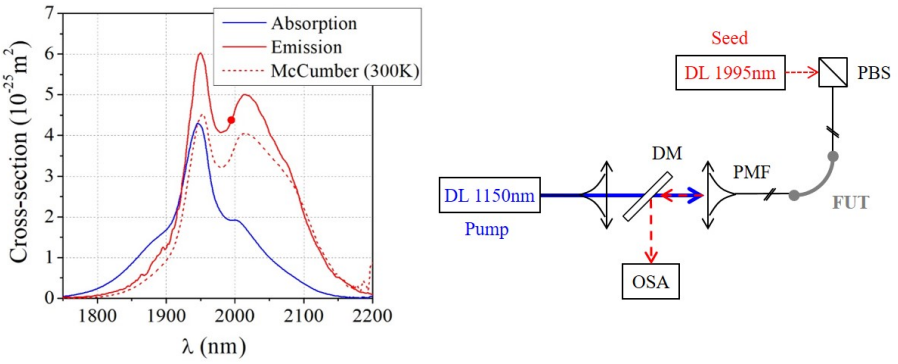

Fig. 1. Left: cross-section spectra for absorption (blue line) and emission (red line) of the Ho doped single mode fiber. The emission spectrum calculated from McCumber equation is displayed in dotted line. The red dot on the emission spectrum indicates the position λ_{test} = 1995 nm where the small-signal gain was measured. Right: setup for the measurement of the small-signal gain (seed on) or the fluorescence spectrum (seed off).

Another HDF-PM-8-130 sample (fiber #2) was prepared with a higher Ho^{3+} concentration. The relative shape of the absorption spectrum is identical to that of the previous sample. The linear absorption of this fiber is 425 ± 5 dB/m at 1950 nm, with the same core diameter and NA=0.21 ($\Gamma(\lambda_0)$ = 0.85). The WDS analysis yields a Ho^{3+} concentration [Ho] = $(27 \pm 1)10^{25}$ m^{-3}. Thanks to the better sensitivity on concentration measurement, the estimation of the absorption cross-section is narrowed down to $\sigma_{\text{abs}}(\lambda_0) = (4.3 \pm 0.2)10^{-25}$ m^2 (see Fig. 1, left).

2.2. Emission cross-section spectrum

The absolute measurement of the emission cross-section spectrum $\sigma_{\text{em}}(\lambda)$ is not straightforward in general and we present here, to the best of our knowledge, its first realization on a holmium doped fiber. The most accurate method to obtain $\sigma_{\text{em}}(\lambda)$ consists in measuring the relative shape $S_{\text{fluo}}(\lambda)$ of the fluorescence spectrum, and determining the absolute emission cross-section at a particular wavelength to scale the whole spectrum. As reminded below, this absolute value can be obtained by measuring the small-signal gain.

In homogeneously broadened transitions such as those involved in the rare-earth doped fiber lasers at room temperature, all the sublevels of all the ions in the excited state contribute to the emission. To make sure that all the possible contributions are taken into account in the fluorescence and gain measurements, the ions were pumped to the $^5I_6$ level. In a silica fiber, the $^5I_8 - {}^5I_6$ transition corresponds to a wavelength of about 1150 nm [23]. We also based this choice of pump wavelength on the optical components that were available to separate the pump and the back-scattered fluorescence (see below). Pumping at 1950 nm is also possible but requires an optimized broadband optical coupler [24].

The setup used to measure the small-signal gain and the fluorescence spectrum is illustrated on Fig. 1 (right). The population inversion is provided by a 1150 nm laser diode that delivers 400 mW on a linear polarization. This pump beam is collimated, transmitted through a standard dichroic mirror (DM: Thorlabs DMSP1500) and coupled into the core of the fiber under test (FUT=fiber #1), which is polarization maintaining (PM). At the FUT output, a fiber coupled polarizing beam splitter (PBS) allows the injection of the small signal, propagating in the opposite direction of the pump, with an orthogonal polarization. The small signal itself consists of about 1 μW at λ_{test} =1995 nm, delivered by a PM fiber coupled laser diode. The fluorescence or amplified signal is redirected by the DM towards an optical spectrum analyzer (OSA).

The length of the FUT must be chosen such that the population is completely inverted along the

sample. A rule of thumb suggests that the sample should be much shorter than the inverse of the holmium absorption $\alpha_{\mathrm{Ho}}(1150\ \mathrm{nm})$. From [17] we find $\alpha_{\mathrm{Ho}}(1950\ \mathrm{nm})/\alpha_{\mathrm{Ho}}(1150\ \mathrm{nm}) \simeq 2$, so for the moderately doped sample (fiber #1) we estimate $\alpha_{\mathrm{Ho}}(1150\ \mathrm{nm}) \simeq 29\ \mathrm{dB/m} \simeq 7\ \mathrm{m}^{-1}$. Thus the FUT should be much shorter than 14 cm to guarantee a complete population inversion along the sample. By shortening the fiber sample from 10 cm to 5 mm, and acquiring the corresponding fluorescence spectra, we find that they become identical for $L_{\mathrm{FUT}} \lesssim 2$ cm. After correction from the transmission spectrum between the FUT and the OSA (lenses, DM, fiber coupling...), we obtain the relative shape of the emission cross-section spectrum.

In order to determine the absolute emission cross-section, we measure the small-signal gain at one particular wavelength λ_{test}. Indeed, the ratio between absorption and emission cross-sections $\sigma_{\mathrm{em}}/\sigma_{\mathrm{abs}}$ at a given wavelength λ is equal to the ratio g^*/α_{Ho} between the corresponding small-signal absorption and gain at λ [22]. Then the peak emission cross-section of the ${}^5I_7 - {}^5I_8$ transition is obtained by the following identity:

$$\frac{\sigma_{\mathrm{em}}^{\mathrm{peak}}}{\sigma_{\mathrm{abs}}^{\mathrm{peak}}} = \frac{\sigma_{\mathrm{em}}^{\mathrm{peak}}}{\sigma_{\mathrm{em}}(\lambda_{\mathrm{test}})} \cdot \frac{\sigma_{\mathrm{em}}(\lambda_{\mathrm{test}})}{\sigma_{\mathrm{abs}}(\lambda_{\mathrm{test}})} \cdot \frac{\sigma_{\mathrm{abs}}(\lambda_{\mathrm{test}})}{\sigma_{\mathrm{abs}}^{\mathrm{peak}}} = \frac{S_{\mathrm{fluo}}^{\mathrm{peak}}}{S_{\mathrm{fluo}}(\lambda_{\mathrm{test}})} \cdot \frac{g^*(\lambda_{\mathrm{test}})}{\alpha_{\mathrm{Ho}}(\lambda_{\mathrm{test}})} \cdot \frac{\alpha_{\mathrm{Ho}}(\lambda_{\mathrm{test}})}{\alpha_{\mathrm{Ho}}^{\mathrm{peak}}} \tag{2}$$

$$= \frac{S_{\mathrm{fluo}}^{\mathrm{peak}}}{S_{\mathrm{fluo}}(\lambda_{\mathrm{test}})} \cdot \frac{g^*(\lambda_{\mathrm{test}})}{\alpha_{\mathrm{Ho}}^{\mathrm{peak}}} \tag{3}$$

where the first ratio is obtained from the measurement of a fluorescence spectrum and yields $S_{\mathrm{fluo}}^{\mathrm{peak}}/S_{\mathrm{fluo}}(\lambda_{\mathrm{test}}) = 1.37$.

The small-signal gain is obtained by comparing the powers at the input and output of the FUT, and taking into account the transmission of all the components or splices that are not common to the two measurements. On a length of 20 mm, where a full population inversion is obtained, we measure a gain of 1.16 ± 0.05 dB, which corresponds to a linear small-signal gain $g^*(\lambda_{\mathrm{test}} = 1995\mathrm{nm}) = 58 \pm 3$ dB/m. By coincidence this value is very similar to the absorption at 1946 nm ($\alpha_{\mathrm{Ho}}^{\mathrm{peak}} = 57 \pm 1$ dB/m), and we find the scaling ratio $\sigma_{\mathrm{em}}^{\mathrm{peak}}/\sigma_{\mathrm{abs}}^{\mathrm{peak}} = 1.40 \pm 0.06$. Given the value of the peak absorption cross-section, we finally estimate the peak emission cross-section to $\sigma_{\mathrm{em}}^{\mathrm{peak}} = 6.0 \pm 0.4\ 10^{-25}\mathrm{m}^2$.

The difference between the peak emission and absorption may seem important, since most of the papers on Ho^{3+}-doped fibers report equal amplitudes at the peak [7,18,25,26]. However these authors calculate the emission cross-section using the well-known McCumber relation, assuming that the absorption and emission spectra are equal at the absorption peak. Two reservations can be expressed against this method, justifying our effort for an absolute measurement.

First the use of the McCumber relation requires an accurate knowledge of the partition function in the ground and excited states of the laser transition [27]. A common method consists in assuming an even splitting between the energy sublevels in these states, and the energy splitting is obtained by dividing the spectral width of the homogeneously broadened transition by the number of sublevels [28]. However, unlike in Kramers ions (e.g. Er^{3+} or Yb^{3+}), the degeneracy of the sublevels of the non-Kramers ions (e.g. Ho^{3+} and Tm^{3+}) can stay high in a host exhibiting a high degree of symmetry (like amorphous silica). In that case the numbers of sublevels to consider depends on the host, so their determination seems hazardous.

Second, the application of the McCumber relation requires that the linewidths ΔE_{ij} of each transition between a Stark sublevel i of the lower manifold and a sublevel j in the upper manifold satisfies the following condition [29, 30]:

$$\Delta E_{\mathrm{ij}} \ll k_{\mathrm{B}} T \tag{4}$$

where k_{B} is the Boltzmann constant and T is the temperature. At room temperature and a central wavelength of 1950 nm, this corresponds to the condition $\Delta\lambda_{\mathrm{ij}} \ll 80$ nm. Considering

for example the zero-phonon transition of the absorption spectrum (see Fig. 1, left), we find a linewidth of about 60 nm. Therefore the condition above is not strictly respected, and the accuracy of the resulting emission cross-section spectra is questionable.

As an illustration, we plot on Fig. 1 (left, dotted line) the emission cross-section $\sigma_{\mathrm{em}}(\lambda)$ calculated with the McCumber relation from $\sigma_{\mathrm{abs}}(\lambda)$, and assuming that the two spectra intersect at the absorption peak wavelength 1946 nm. The figure does illustrate a noticeable difference close to the peak, but also that the measured and calculated spectra almost overlap beyond 2100 nm. This probably explains why the McCumber calculation of the emission cross-section spectra do not totally alter the accuracy of laser simulations, at least for $\lambda > 2100$ nm. Eventually, let us remind that our value of emission cross-section seems to be the first report from a direct measurement, instead of indirect calculations.

2.3. Laser excited state lifetime

The setup for the measurement of the $^5I_7$ level lifetime is very similar to that of the emission cross-section [22]. However, the timescale of the fluorescence decay (on the order of 1 ms) requires a detection system with a faster rise time than the OSA, hence a smaller detection area, and a lower signal intensity. The power delivered by the 1150 nm laser diode appeared too low compared to the detection noise of our photodiode, so we built a Yb-doped fiber laser, based on the design described in [31]. With the pump diodes that were available, we managed to generate a power of about 1 W at 1150 nm, sufficient to pump a 10 cm sample of fiber #1.

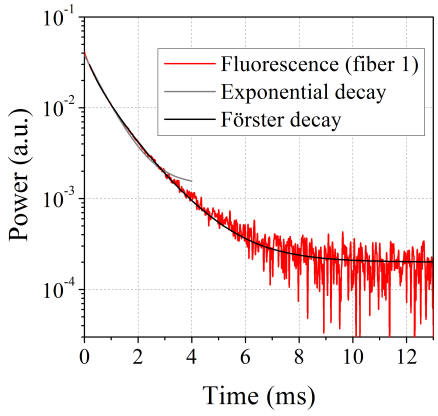

Fig. 2. Temporal decay of the fluorescence from the $^5I_7$ excited level, after optical pumping in the $^5I_6$ level. The experimental curve is fitted with two functions: the common single exponential decay (gray), as well as the non-exponential Förster decay function (black). The better fit of the latter illustrates the onset of energy transfers between adjacent excited holmium ions.

In order to alternate population inversion and observation of fluorescence decay, we apply a 100 Hz square modulation on the pump power by adding a free-space acousto-optical modulator (AOM) on the path of the 1150 nm beam. In absence of Ho doped fiber, we find that the detection response time is about 10 µs. The result of an averaging with the FUT is illustrated on Figure 2. The non-exponential decay can be a sign of energy transfers between adjacent Ho^{3+} ions, typically through dipolar coupling [32]. In that case the experimental curve can be well described by a Förster decay function [33] :

$$P(t) = P_0 + A.\exp\left(-\gamma\sqrt{t} - t/\tau_0\right) \tag{5}$$

The fit yields here the following parameters: $\tau_0 = 1.9$ ms and $\gamma = 34$ s$^{-1/2}$. A detailed modeling of the influence of the energy transfers between adjacent ions is out of the scope of this study. We thus let aside the modification of the rate equations, and consider that the decay of the excited state is described by one effective lifetime.

Fitting the first part of the fluorescence signal (until about 4 µs) with a single exponential decay yields a value of 0.7 ± 0.1 ms, which agrees with the value generally reported [25, 34]. The agreement between measurements and simulation, illustrated in the next sections, tends to suggest that this approximation does not alter notably the accuracy of the model.

2.4. Background loss and hydroxyl concentration

The attenuation at pump and signal wavelengths is a critical parameter for fiber sources, especially in a clad pumping configuration where the fiber can extend to more than 10 m to absorb the pump. In the spectral domain close to 2 µm, where our pump and signal beams lie, the hydroxyl groups OH bound to the silica network present absorption peaks due to rovibrational transitions. A crucial concern in the realization of holmium doped optical fibers must be the reduction of the OH concentration, to optimize the laser efficiency.

The holmium doped core material was manufactured using a solution doping technology. The process consists in soaking a porous silica layer with a solution containing dissolved Ho^{3+} and Al^{3+} ions. Despite the use of water in the process, a low OH content can be obtained by taking appropriate precautions. The porous silica layer must be deposited using a well maintained MCVD equipment fitted with high purity precursors.In such conditions, silica with OH content lower than 50 ppb can be obtained routinely. Once the porous layer has been soaked and the solution drained away, the subsequent drying procedure must include a chlorination step at high temperature to remove any moisture trace, prior to vitrification and collapse. Provided this drying step is well designed, no additional OH content is observed.

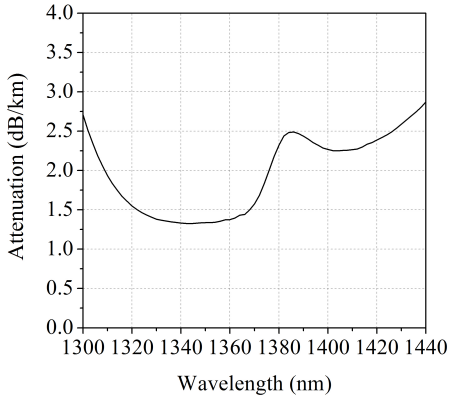

Fig. 3. Attenuation spectrum measured on a 233 m sample of Ho-doped fiber (fiber #1) close to 1380 nm, in order to estimate the concentration of OH groups.

According to the values reported in [14], the linear attenuation relative to OH concentration is about 60 dB/km/ppm close to 1380 nm, wavelength of the first overtone of an OH fundamental stretching vibration. We measure the linear attenuation spectrum of a 233 m sample of fiber #1 around this wavelength, using the usual cut-back method. The result of this measurement is presented on Figure 3. As expected, a distinct peak appears at 1380 nm, showing an attenuation of about 2.5 dB/km. The corresponding OH concentration can be estimated to about 0.04 ppm, and the contribution of OH to the attenuation at the laser wavelength is lower than 1 dB/km. This value is remarkably low compared to the 1 ppm reported in [18] or even the previous record low

value of 0.14 ppm reported in [7]. As discussed in section 4, such a glass purity is an important requirement in the race for efficient fiber lasers in this spectral domain.

2.5. Pair induced non-saturable absorption

Another notable contribution to the attenuation of pump and signal is due to the formation of rare-earth ion pairs in highly doped fibers [17]. The electronic structure of the holmium ion, like in erbium or thulium, allows transfers of energy between ions in close vicinity. The pair induced quenching (PIQ) typically alters the pumping efficiency of a fiber laser, and can also affect the transmission of the amplified signal [35]. When the pump or signal power is very high compared to the saturation power of the corresponding transition, one of the ions of a pair in the excited state decays non-radiatively to the ground state while the other is up-converted to a higher energy level. This non-saturable absorption thus translates into a loss mechanism for both signal and pump beams.

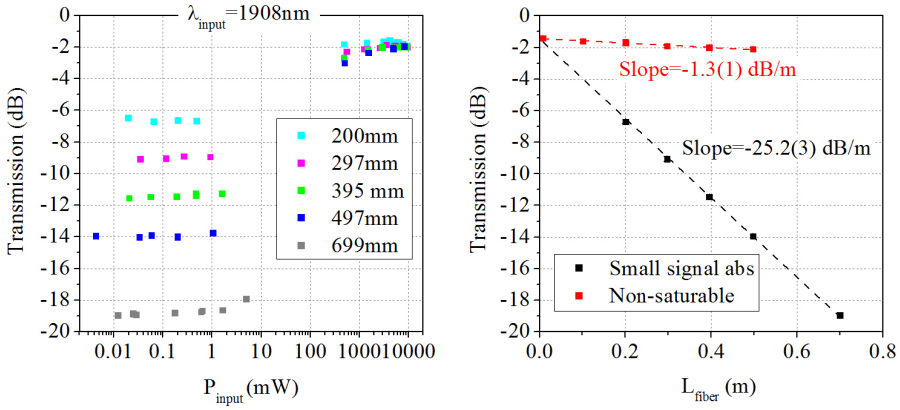

Fig. 4. Left: transmissions of various lengths of the FUT, as a function of the input power P_{in} at $\lambda_{\text{in}} = 1908$ nm. Right: Evolution of the small-signal ($P_{\text{in}} < 1$ mW) and non-saturable ($P_{\text{in}} > 1$ W) transmissions as a function of the FUT length.

As it is well-known, a codoping of alumina (Al) is necessary to separate the rare-earth ions and reduce the formation of ion pairs [17, 24]. During the fabrication process of the preform that leads to fiber #1, the atomic ratio Al/Ho is about 40.

The non-saturable absorption is measured by varying the power injected into the FUT, in the spectral band of the laser transition, following a standard method [36]. As a probe source, we use a Tm-doped fiber laser at $\lambda_{\text{in}} = 1908$ nm (IPG TLR10-1908-LP). Its nearly gaussian beam is coupled into a short piece of single-mode PM1950 fiber, which is fused to a sample of fiber #1. The initial length of the sample for this measurement is about 0.7 m. For input powers lower than 10 mW, the output power is measured with a pyroelectric detector, and we use a calorimeter for input powers higher than a few hundreds of mW.

We report on Fig. 4 (left) the transmission as a function of the input power, for several length L_{FUT} of fiber #1. This figure clearly illustrates the two regimes of small-signal transmission T_{Ho} (for $P_{\text{input}} < 1$ mW) and saturated transmission T_{sat} (for $P_{\text{input}} > 1$ W). Obviously these transmission values are biased with various losses, but they are independent of the FUT length (transmissions of fiber components, splices at the input/output of the FUT...). The asymptotic values T_{Ho} and T_{sat} obtained as a function of L_{FUT} are plotted on Fig. 4 (right) and fitted with lines. The intercept at $L_{\text{FUT}} = 0$ corresponds to the constant loss contribution, of about 2 dB. From the slopes t of the two linear fits, we deduce the corresponding small-signal absorption $\alpha_{\text{Ho}} = -t_{\text{Ho}}$ and non-saturable absorption $\alpha_{\text{ns}} = -t_{\text{ns}}$ of holmium in this sample. In the case of

fiber #1, we find $\alpha_{\mathrm{Ho}}(\lambda_{\mathrm{in}}) = 25.2 \pm 0.3$ dB/m and $\alpha_{\mathrm{ns}}(\lambda_{\mathrm{in}}) = 1.3 \pm 0.1$ dB/m.

These two values are related to the fraction $2k$ of ions in pairs by the expression derived in [37]:

$$\alpha_{\mathrm{ns}}(\lambda) = 2k \cdot \alpha_{\mathrm{Ho}}(\lambda) \cdot \left[1 - \frac{\sigma_{\mathrm{abs}}(\lambda) + \sigma_{\mathrm{em}}(\lambda)}{2\sigma_{\mathrm{abs}}(\lambda) + \sigma_{\mathrm{em}}(\lambda)}\right] \tag{6}$$

where $\sigma_{\mathrm{abs}}(\lambda)$ and $\sigma_{\mathrm{em}}(\lambda)$ are the absorption and emission cross-section spectra reported above (see Fig. 1). Considering the cross-sections at $\lambda_{\mathrm{in}} = 1908$ nm ($\sigma_{\mathrm{abs}} = 1.9\ 10^{-25}\mathrm{m}^2$ and $\sigma_{\mathrm{em}} = 1.6\ 10^{-25}\mathrm{m}^2$), we find that $2k = 15 \pm 1\%$. Here again, the literature is very scarce about direct measurements of ion pairs concentration. Our value is comparable with the very few measurements reported on holmium doped fibers with similar holmium concentration [17, 38].

3. Realization and analysis of a high power laser

Our short-term objective is to study the ultimate efficiency and maximum power of an all-fiber holmium laser, so we focus here on the laser oscillator configuration. Future works will be dedicated to the single-frequency amplifier configuration. Both experimental results and simulation analysis of the fiber laser are presented.

3.1. Fiber laser setup

Our setup illustrated on Fig. 5 is a standard oscillator configuration, based on a LMA triple-clad holmium doped fiber (IXF-3CF-Ho-O-20-250-300-0.08, see insert in Fig. 5). The triple clad (3CF) structure, also named all-glass cladding, is now familiar in reports on in-band pumped fibers emitting in the 2 µm spectral range [7, 10, 39]. The active core ($D_{\mathrm{core}} = 20$ µm) is surrounded by a Ge-doped pedestal ($D_{\mathrm{ped}} = 64$ µm) that guarantees a low numerical aperture of 0.08. The pump is guided in the pure silica cladding ($D_{\mathrm{clad1}} = 250$ µm flat to flat), thanks to a surrounding layer of fluorine (F) doped silica ($D_{\mathrm{clad2}} = 300$ µm). This interface is shaped as an octagon, in order to break the angular symmetry and force the pump beam to cross the doped core. Due to the limitation in F concentration, the numerical aperture of the pump guiding interface cannot be much higher than 0.22. The mechanical protection of the fiber is ensured by a polymer cladding, resulting in a total external diameter $D_{\mathrm{clad3}} = 450$ µm. A passive 3CF with identical core and clad diameters and NA is also drawn, to bear the fiber Bragg grating (see below). The clad of the passive 3CF is circular instead of octagonal.

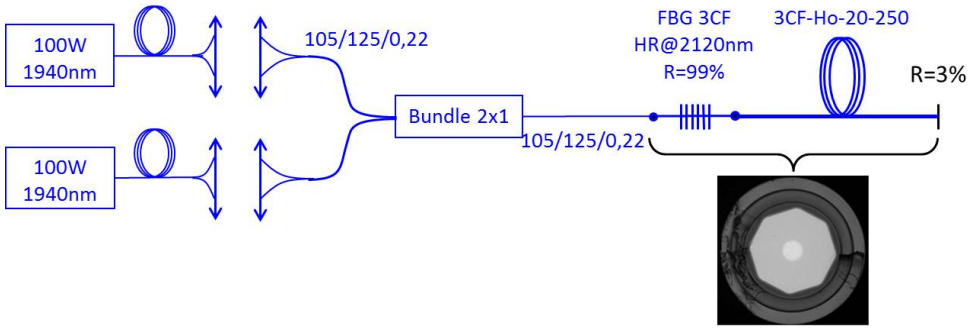

Fig. 5. Design of the holmium-doped fiber laser configuration. The insert illustrates the triple-clad structure of the active fiber (3CF-Ho). The passive fiber of the FBG is also a 3CF, with a circular cladding.

The absorption by the holmium ions in the 3CF is measured by a cut-back method on a sample of initial length 1.5 m. We succeed in keeping the fraction of light coupled into the pedestal lower than 1%, and find a core absorption of 86±3 dB/m at the peak absorption wavelength 1946 nm for

the fundamental guided mode. The ion concentration was estimated to about 5.3 10^{25} m^{-3}, from the quantity of holmium oxyde introduced during the preform fabrication. Using eq. (1) and taking into account the overlap $\Gamma = 84\%$ between doped core and optical mode, this estimation yields an absorption $\alpha_{\mathrm{Ho}}^{\mathrm{peak}} \simeq 20\ \mathrm{m}^{-1} = 87$ dB/m, which is consistent with the value measured directly in the fiber for the fundamental mode.

The highly reflective mirror is a fiber Bragg grating (FBG) written in the passive 3CF fiber with same dimensions and NA as the 3CF-Ho fiber. The FBG is manufactured by iXblue using a proprietary process that allows a minimal heating at high power for $\lambda_s = 2120$ nm. Its reflectivity is about 99% at λ_s, with a 3 dB linewidth of 2 nm. The laser cavity output coupler is obtained by the flat cleaved end facet of the active fiber. The Fresnel reflectivity of this silica-air interface is approximately 3%.

The pump light is provided by two commercial fiber lasers delivering collimated single-mode beams (M^2<1.05) with a power up to 120 W each at 1940 nm, in a linewidth lower than 1 nm. The two beams are focused through AR coated dry-silica lenses (Corning 7979) into the multimode fibers (MMF: 105/125/0.22) of a 2x1 pump combiner. The output port of the combiner is an identical MMF fiber. It is then spliced to the passive 3CF with the core-engraved FBG, which is spliced itself to the 3CF-Ho active fiber. Between the free-space output of the commercial pump lasers, and the output of a 5 cm length of the 3CF-Ho fiber, we measured a transmission of 93±1% for both pump beams. This value corresponds to the following sequence for the pump beams: focusing lens / injection in the input MMF of the combiner / 2x1 combiner / combiner MMF output - passive 3CF with FBG splice/ passive 3CF - Ho-3CF splice.

The 3CF-Ho is cooled by a small fan blowing above. The fiber output beam, carrying the laser signal and the residual pump, is collimated with another dry-silica lens. The material and AR-coating of the lenses allow a transmission higher than 99% at the pump and signal wavelengths. A dichroic filter transmits the residual pump (T=95% at λ_p) and reflects the laser signal (R=99% at λ_s). The output power at both wavelengths is measured by calorimeters on each side of the filter. A fraction of the signal port is also coupled into an optical spectrum analyzer.

3.2. Experimental results

Using our numerical model described below, with the parameters reported in Section 2, we first estimated the fiber length required to maximize the signal power to about L≃16 m. We then tested the laser efficiency with this fiber length. The evolution of the signal power as a function of the pump power is shown on Fig. 6 (left).

For the maximum coupled pump power of about 200 W, the laser delivers an output power of 90 W at 2120 nm. The optical efficiency, defined as the slope of the signal power as a function of the coupled pump power, reaches 49%. As a comparison, the maximum output power reported at this wavelength from a Ho fiber laser in the same configuration is about 400 W, for a 1 kW pump power [6]. Up to a pump power of 400 W, the laser efficiency was slightly lower than 50%.

The efficiency that we report is identical, despite a fundamental difference. Indeed, the overlap between the pump beam and the active region in our fiber is much less favourable. The Ho-doped fiber presented here results from the first trials of 3CF manufacturing at iXblue. Due to the difficulties of filling properly a big preform core and machining a small preform, the clad diameter of our fiber could not be reduced to less than 250 µm, instead of 112 µm for the Nufern fiber of the DSTG [18]. Therefore the pump/core overlap in our fiber is lower by more than a factor of 4, which reduces the thermal load. The corollary drawback is that for a comparable Ho concentration, our fiber length must be much longer, thus increasing the loss on the pump and signal fields and altering the laser efficiency. The lower OH concentration and pair fraction of our fiber allows however a state of the art efficiency. As described in the next section, this performance is well understood in light of our numerical model.

The laser spectrum is monitored on the OSA as the laser signal power increases, with a

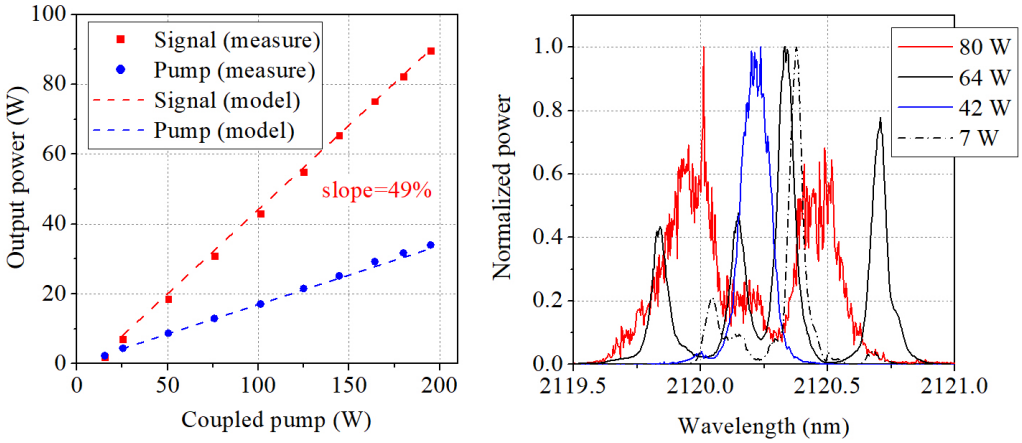

Fig. 6. Left: evolution of the output signal and residual pump powers (respectively red and blue), as a function of the pump power. The dots represent the experimental data, the lines the result of our simulation. Right: Signal spectra for various values of P_{sig}, for a resolution 0.05 nm.

resolution of 0.05 nm. As illustrated on Fig. 6 (right), the bandwidth remains in the range of 1 nm, as defined by the FBG, up to the maximum laser power. More importantly, one can see that the center wavelength does not increase, as could be the case for example if the thermal load expands the grating. As for the shape of the spectrum at 80 W, the high resolution of the OSA allows the observation of a sharper aspect. Numerous longitudinal modes oscillate in the long fiber cavity, and the result of their competition can vary rapidly. The sharper shape may result from variations of the spectrum on a time scale close to that of the OSA sweep time. The study of the spectrum shape is out of the scope of this paper but will be investigated in later works.

Finally, the laser was tested for a fiber length of 10 m, in order to check the influence of fiber length on the efficiency. In that case, the laser power was 70 W at 2120 nm, for a pump power of 170 W, and the optical efficiency was 43%. These values are also in good agreement with the model presented below.

3.3. Comparison with numerical modeling

The powers at the laser signal and pump wavelength are calculated along the fiber path by solving the usual rate and propagation equations [22,40], with the common approximation of the effective overlap integral between the active region and the propagating mode to suppress the radial dependence [15]. We describe the holmium amplifying medium as a simple homogeneously broadened two-level system, considering only the ${}^5I_8 - {}^5I_7$ transition.

The numerical model takes into account the physical parameters of the fiber (core/clad diameters and NA), as well as the data that we measured and reported in Section 2. The main values required for the simulation are listed in Table 1.

The fraction of ions in pairs $2k$ could not be measured directly on the 3CF-Ho LMA fiber, but we can estimate it from the value that was measured in the fiber #1 ($2k = 15\%$ for $\alpha_{\mathrm{Ho}}^{\mathrm{peak}} = 57$ dB/m). Assuming a proportional variation around these absorption values, we expect $2k = 23\%$. Note that the ratio of atomic contents Al/Ho for this preform was also close to 40. The effect of PIQ on the laser efficiency is modeled in a simple way, since the powers involved are much higher than the saturation power $P_{\mathrm{sat}} = h\nu A_{\mathrm{core}}/(\sigma_{\mathrm{abs}} + \sigma_{\mathrm{em}})\Gamma\tau_0$, at both λ_p and λ_s (about 40 mW and 260 mW respectively). The attenuation induced by the ion pairs at λ_p and λ_s is thus essentially constant along the fiber and can be identified to the non-saturable absorption at these wavelengths

Table 1. List of the parameters of the Ho-doped fiber laser used in the numerical simulation

Parameter	Value	Comment
D_{core}	20 µm	Core diameter
D_{clad1}	250 µm	Pump clad diameter
NA_{core}	0.08	Numerical aperture
τ_0	0.7 ms	Laser transition fluorescence lifetime
$\alpha_{\text{Ho}}^{\text{peak}}$	86 dB/m	Ho^{3+} peak absorption at 1946 nm
$2k$	23%	Fraction of Ho^{3+} ions in pairs
$\zeta_{\text{clad}}(\lambda_p)$	10 dB/km	Pump attenuation in the clad (OH and multi-phonon)
$\zeta_{\text{core}}(\lambda_s)$	40 dB/km	Signal attenuation in the core (mainly multi-phonon)

(eq. 6). For the signal propagating in the core, the contribution $\alpha_{\text{ns}}(\lambda_s)$ is added directly to the attenuation $\zeta_{\text{core}}(\lambda_s)$, while for the pump propagating in the clad, the term $\alpha_{\text{ns}}(\lambda_p)$ must be weighted by the surface ratio $A_{\text{core}}/A_{\text{clad}}$ between core and clad before addition to $\zeta_{\text{clad}}(\lambda_p)$.

For the pump beam, another cause of attenuation can originate from the hydroxyl concentration at the octagon interface between the fluorinated outer cladding and the pure silica inner cladding. In order to obtain the 3CF preform, we first realize a primary silica preform (containing the Ho-doped core), which is then sleeved inside a tube that contains an inner layer doped with fluorinated silica. During the collapse step of the primary preform, by burners in open-air, the external layer is highly contaminated by OH groups. However the chemical and mechanical etching that we use, to obtain the octagon shape, eliminates the external skin that contains the OH groups. As presented in a recent paper that compares the residual OH concentration by mechanical or CO_2 laser shaping, the attenuation at 1.38 µm is lower than 130 dB/km with a mechanical technique [41]. At λ_p, the attenuation would thus be about 6 dB/km [14]. Since we make sure to remove more silica from the primary preform than our estimation of OH diffusion depth, we consider this value as an upper bound of OH attenuation for our 3CF clad.

The only parameter that could not be derived from the measurements on the Ho-doped fiber is the contribution to the silica attenuation from the multi-phonon absorption ζ_{silica} by the SiO_4 bonds. Therefore we consider $\zeta_{\text{silica}}(\lambda_s)$ as a parameter to fit the numerical simulation to the experimental result for the output signal power. The best fit between measurement and simulation is obtained for $\zeta_{\text{silica}}(\lambda_s) = 40$ dB/km. This value is of the same order as those reported in the literature [42, 43]. Given the typical ratio $\zeta_{\text{silica}}(\lambda_s)/\zeta_{\text{silica}}(\lambda_p) \simeq 10$ between this attenuation at our pump and signal wavelengths [18], we consider the estimation $\zeta_{\text{silica}}(\lambda_p) \simeq 4$ dB/km. The results of the simulation for the signal and pump powers at the fiber output are displayed as the dotted lines (red and blue respectively) on Fig. 6 (left), as a function of the coupled pump power.

We note that the value of $2k$ estimated for our fiber, and validated by our model, is notably lower than the value $2k = 30\%$ inferred in [40] for the fiber tested in [6], with a lower peak absorption of 70 dB/m. However the direct comparison is not relevant, since the fraction of paired ions is known to be highly dependent on the host composition [38, 44–46]. The evolution of $2k$ as a function of the Ho^{3+} concentration in our silica hosts is the subject of an ongoing work.

4. Discussion on the power limitation

We now use our model to illustrate the role of the two main causes of attenuation in the Ho-doped core, namely OH groups and holmium pairs. For holmium doped fibers, the literature shows that

the concentration [OH] ranges typically between 0.01 ppm and 10 ppm. As for the fraction of ions in pair $2k$, it can reach 30% [40], and we suppose that it could be reduced down to 20%. Considering a fiber with the dimensions and parameters listed in Table 1, the simulation is run for various values of [OH] and $2k$. For each pair of these parameters, we calculate the maximum laser slope efficiency, looking for the optimal fiber length (Fig. 7).

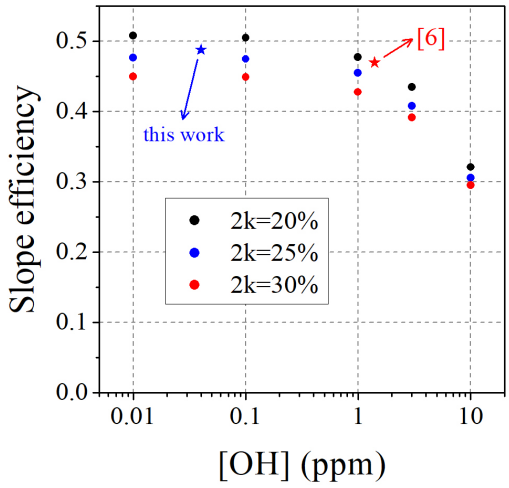

Fig. 7. Influence of the concentration of OH groups on the efficiency of a fiber laser, with the parameters listed in Table 1, for various values of fraction $2k$ of Ho^{3+} ions in pairs. The blue and red stars represent respectively the efficiencies of our fiber laser, and of the laser reported in [6] (for P_{signal} up to $\simeq 200\ W$).

We find that for a given value of $2k$, reducing [OH] from 1 ppm to 0.1 ppm improves the slope efficiency by less than 3% percent, while the same improvement can be obtained by reducing $2k$ from 30% to 25%. This first observation shows that for [OH] lower than 1 ppm, the main effort should lie rather on avoiding the ion pairs than on reaching a dryer silica core. The dilution of the Ho^{3+} ions hence appears as the main concern in the design of future fibers, as shows the resurgence of interest for nanoparticle doping [24, 46, 47].

Finally, we used our simulation tool to study the holmium doped fiber that still holds the highest laser power published to date [6], using the values gathered in [40]. For the contribution of the ion pairs, we identify it again to the non-saturable absorption, using the value $2k = 30\%$ that was inferred from the comparison between model and experimental results [40]. With this approximation, we find for example $P_s = 183$ W for $P_p = 400$ W, and a slope efficiency of 47%, both values in excellent agreement with the experimental data. The agreement suggests that our model, with the approximations mentioned above, yields the same accuracy as the complete model presented in [38, 40].

5. Conclusion

We report here on the study of a holmium doped fiber laser for the high power continuous regime, using triple-clad fibers adapted to the in-band pumping in the 2 µm band. One interest of our work lies in the detailed spectroscopy of the laser transition of the holmium ion in a silica host: lifetime, interaction cross-section spectra, fraction of Ho^{3+} pairs... We also demonstrate a laser efficiency of about 50%, which corresponds to the present state of the art for a all-fiber clad-pumped laser in the 100 W class. Another major aspect of this study is the comparison with the numerical simulation that uses the values obtained from the spectroscopy measurements. The

agreement of our simulation with the experiment shows that it provides a good understanding of the laser system. It will thus be useful to design more efficient Ho-doped fibers for high power laser sources emitting at $\lambda > 2.1$ µm. Further work is now in preparation to improve the laser efficiency and describe more precisely the role of PIQ.

Acknowledgments

The authors are thankful to the french defense direction DGA for financial support.

Disclosures

The authors declare no conflicts of interest.

References

1. J. Zhang, V. Fromzel, and M. Dubinskii, "Resonantly cladding-pumped Yb-free Er-doped LMA fiber laser with record high power and efficiency," Opt. Express **19**, 5574–5578 (2011).
2. R. Liang, J. Chen, G. Kipshidze, D. Westerfeld, L. Shterengas, and G. Belenky, "High-power 2.2-μm diode lasers with heavily strained active region," Photonics Technol. Lett. IEEE **23**, 603 – 605 (2011).
3. G. D. Goodno, L. D. Book, and J. E. Rothenberg, "Low-phase-noise, single-frequency, single-mode 608 W thulium fiber amplifier," Opt. Lett. **34**, 1204–1206 (2009).
4. T. Ehrenreich, R. Leveille, I. Majid, K. Tankala, G. Rines, and P. F. Moulton, "1kW, all-glass Tm:fiber laser," in *proc. SPIE Photonics West,* (2010).
5. A. Sincore, J. D. Bradford, J. Cook, L. Shah, and M. C. Richardson, "High average power thulium-doped silica fiber lasers: Review of systems and concepts," IEEE J. Sel. Top. Quantum Electron. **24**, 1–8 (2018).
6. A. Hemming, N. Simakov, A. Davidson, S. Bennetts, M. Hughes, N. Carmody, P. Davies, L. Corena, D. Stepanov, J. Haub, R. Swain, and A. Carter, "A monolithic cladding pumped holmium-doped fibre laser," in *CLEO: 2013,* (Optical Society of America, 2013), p. CW1M.1.
7. E. J. Friebele, C. G. Askins, J. R. Peele, B. M. Wright, N. J. Condon, S. O'Connor, C. G. Brown, and S. R. Bowman, "Ho-doped fiber for high energy laser applications," in *Proc. SPIE,* vol. 8961 (2014), p. 896120.
8. J. Aubrecht, P. Peterka, P. Honzatko, Y. Baravets, M. Jelinek, V. Kubecek, M. Pawliszewska, J. Sotor, G. Sobon, K. M. Abramski, and I. Kasik, "Characterization of holmium fibers with various concentrations for fiber laser applications around 2.1 um," in *Proc. SPIE,* vol. 9886 (2016), p. 988607.
9. A. M. Sincore, L. Shah, V. Smirnov, and M. C. Richardson, "Comparison of in-band pumped Tm:fiber and Ho:fiber," in *Proc. SPIE,* vol. 9728 (2016), p. 972830.
10. P. C. Shardlow, N. Simakov, A. Billaud, J. M. O. Daniel, P. Barua, J. Sahu, A. Hemming, and W. A. Clarkson, "Holmium doped fibre optimised for resonant cladding pumping," in *2017 European Conference on Lasers and Electro-Optics and European Quantum Electronics Conference,* (Optical Society of America, 2017), p. CJ_11_4.
11. L. G. Holmen and G. Rustad, "Linearly polarized holmium-doped fiber amplifier at 2.11 μm," in *Europhoton,* (2018), p. ThP.9.
12. C. C. Baker, E. J. Friebele, A. A. Burdett, L. B. Shaw, S. R. Bowman, W. Kim, J. S. Sanghera, J. M. Ballato, C. Kucera, A. Vargas, A. V. Hemming, N. Simikov, and J. Haub, "Recent advances in holmium doped fibers for high-energy lasers (Conference Presentation)," in *Laser Technology for Defense and Security XIV,* vol. 10637 M. Dubinskiy and T. C. Newell, eds., International Society for Optics and Photonics (SPIE, 2018).
13. A. Hemming, S. Bennetts, N. Simakov, A. Davidson, J. Haub, and A. Carter, "High power operation of cladding pumped holmium-doped silica fibre lasers," Opt. Express **21**, 4560–4566 (2013).
14. O. Humbach, H. Fabian, U. Grzesik, U. Haken, and W. Heitmann, "Analysis of OH absorption bands in synthetic silica," J. Non-Crystalline Solids **203**, 19 – 26 (1996).
15. C. Giles and E. Desurvire, "Modeling erbium doped fiber amplifiers," J. Light. Technol. **9**, 271–283 (1991).
16. J. L. Wagener, P. F. Wysocki, M. J. F. Digonnet, H. J. Shaw, and D. J. DiGiovanni, "Effects of concentration and clusters in erbium-doped fiber lasers," Opt. Lett. **18**, 2014–2016 (1993).
17. A. S. Kurkov, E. M. Sholokhov, A. V. Marakulin, and L. A. Minashina, "Effect of active-ion concentration on holmium fibre laser efficiency," Quantum Electron. **40**, 386–388 (2010).
18. N. Simakov, A. Hemming, W. A. Clarkson, J. Haub, and A. Carter, "A cladding-pumped, tunable holmium doped fiber laser," Opt. Express **21**, 28415–28422 (2013).
19. X. Wang, L. Hu, W. Xu, S. Wang, L. Zhang, C. Yu, and D. Chen, "Spectroscopic properties of Ho^{3+} and Al^{3+} co-doped silica glass for 2-μm laser materials," J. Lumin. **166**, 276 – 281 (2015).
20. N. Simakov, Z. Li, Y. Jung, J. M. O. Daniel, P. Barua, P. C. Shardlow, S. Liang, J. K. Sahu, A. Hemming, W. A. Clarkson, S.-U. Alam, and D. J. Richardson, "High gain holmium-doped fibre amplifiers," Opt. Express **24**, 13946–13956 (2016).
21. P. A. Ryabochkina, A. N. Chabushkin, A. F. Kosolapov, and A. S. Kurkov, "Absorption and luminescence characteristics of $^5I_7 \leftrightarrow ^5 I_8$ transitions of the holmium ion in Ho^{3+}-doped aluminosilicate preforms and fibres," Quantum Electron. **45**, 102–104 (2015).

22. E. Desurvire, *Erbium-Doped Fiber Amplifiers: Principles and Applications* (Wiley, 1994).
23. S. D. Jackson, F. Bugge, and G. Erbert, "Directly diode-pumped holmium fiber lasers," Opt. Lett. **32**, 2496–2498 (2007).
24. M. Kamrádek, I. Kašík, J. Aubrecht, J. Mrázek, O. Podrazký, J. Cajzl, P. Vařák, V. Kubeček, P. Peterka, and P. Honzátko, "Nanoparticle and solution doping for efficient holmium fiber lasers," IEEE Photonics J. **11**, 1–10 (2019).
25. S. R. Bowman, S. O'Connor, N. J. Condon, E. J. Friebele, W. Kim, B. Shaw, and R. S. Quimby, "Non-radiative decay of holmium-doped laser materials," in *Proc. SPIE,* vol. 8638 (2013).
26. X. Fan, P. Kuan, K. Li, L. Zhang, D. Li, and L. Hu, "Spectroscopic properties and quenching mechanism of 2 μm emission in ho3+ doped germanate glasses and fibers," Opt. Mater. Express **5**, 1356–1365 (2015).
27. M. J. F. Digonnet, E. Murphy-Chutorian, and D. G. Falquier, "Fundamental limitations of the McCumber relation applied to Er-doped silica and other amorphous-host lasers," IEEE J. Quantum Electron. **38**, 1629–1637 (2002).
28. W. J. Miniscalco and R. S. Quimby, "General procedure for the analysis of Er^{3+} cross sections," Opt. Lett. **16**, 258–260 (1991).
29. D. E. McCumber, "Einstein relations connecting broadband emission and absorption spectra," Phys. Rev. **136**, A954–A957 (1964).
30. C. Florea and K. A. Winick, "Ytterbium-doped glass waveguide laser fabricated by ion exchange," J. Light. Technol. **17**, 1593 (1999).
31. Y. Miao, H. Zhang, H. Xiao, P. Zhou, and Z. Liu, "1150-nm Yb-doped fiber laser pumped directly by laser-diode with an output power of 52 W," IEEE Photonics Technol. Lett. **26**, 2327–2329 (2014).
32. L. Gomes, V. Fortin, M. Bernier, R. Vallée, S. Poulain, M. Poulain, and S. D. Jackson, "The basic spectroscopic parameters of Ho^{3+}-doped fluoroindate glass for emission at 3.9 μm," Opt. Mater. **60**, 618 – 626 (2016).
33. O. Svelto, *Interaction of Radiation with Atoms and Ions* (Springer US, 2010), chap. 2, 5th ed.
34. D. Hanna, R. Percival, R. Smart, J. Townsend, and A. Tropper, "Continuous-wave oscillation of holmium-doped silica fibre laser," Electron. Lett. **25**, 593–594(1) (1989).
35. E. Delevaque, T. Georges, M. Monerie, P. Lamouler, and J.-F. Bayon, "Modeling of pair-induced quenching in erbium-doped silicate fibers," IEEE Photonics Technol. Lett. **5**, 73–75 (1993).
36. D. Boivin, T. Föhn, E. Burov, A. Pastouret, C. Gonnet, O. Cavani, C. Collet, and S. Lempereur, "Quenching investigation on new erbium doped fibers using MCVD nanoparticle doping process," in *Proc. SPIE,* vol. 7580 (2010), pp. 7580 – 7580 – 9.
37. P. Myslinski, D. Nguyen, and J. Chrostowski, "Effects of concentration on the performance of erbium-doped fiber amplifiers," J. Light. Technol. **15**, 112–120 (1997).
38. J. Wang, N. Bae, S. B. Lee, and K. Lee, "Effects of ion clustering and excited state absorption on the performance of ho-doped fiber lasers," Opt. Express **27**, 14283–14297 (2019).
39. A. Hemming, S. Bennetts, N. Simakov, J. Haub, and A. Carter, "Development of resonantly cladding-pumped holmium-doped fibre lasers," in *Proc. SPIE,* vol. 8237 (2012), p. 82371J.
40. J. Wang, D. Yeom, N. Simakov, A. Hemming, A. Carter, S. B. Lee, and K. Lee, "Numerical modeling of in-band pumped Ho-doped silica fiber lasers," J. Light. Technol. **36**, 5863–5880 (2018).
41. A. A. Jasim, O. Podrazký, P. Peterka, M. Kamrádek, I. Kašík, and P. Honzátko, "Impact of shaping optical fiber preforms based on grinding and a co2 laser on the inner-cladding losses of shaped double-clad fibers," Opt. Express **28**, 13601–13615 (2020).
42. T. Izawa, N. Shibata, and A. Takeda, "Optical attenuation in pure and doped fused silica in the ir wavelength region," Appl. Phys. Lett. **31**, 33–35 (1977).
43. I. Garrett and C. J. Todd, "Components and systems for long-wavelength monomode fibre transmission," Opt. Quantum Electron. **14**, 95–143 (1982).
44. K. Arai, H. Namikawa, K. Kumata, T. Honda, Y. Ishii, and T. Handa, "Aluminum or phosphorus co-doping effects on the fluorescence and structural properties of neodymium-doped silica glass," J. Appl. Phys. **59**, 3430–3436 (1986).
45. N. V. Kiritchenko, L. V. Kotov, M. A. Melkumov, M. E. Likhachev, M. M. Bubnov, M. V. Yashkov, A. Y. Laptev, and A. N. Guryanov, "Effect of ytterbium co-doping on erbium clustering in silica-doped glass," Laser Phys. **25**, 025102 (2015).
46. I. Savelii, L. Bigot, B. Capoen, C. Gonnet, C. C. E. Burova, A. Pastouret, H. El-Hamzaoui, and M. Bouazaoui, "Benefit of rare-earth "smart doping" and material nanostructuring for the next generation of er-doped fibers," Nanoscale Res. Lett. **12** (2017).
47. C. C. Baker, E. J. Friebele, A. A. Burdett, D. L. Rhonehouse, J. Fontana, W. Kim, S. R. Bowman, L. B. Shaw, J. Sanghera, J. Zhang, R. Pattnaik, M. Dubinskii, J. Ballato, C. Kucera, A. Vargas, A. Hemming, N. Simakov, and J. Haub, "Nanoparticle doping for high power fiber lasers at eye-safer wavelengths," Opt. Express **25**, 13903–13915 (2017).